Computers & Fluids 65 (2012) 35–43

Contents lists available at SciVerse ScienceDirect

Computers & Fluids

journal homepage: www.elsevier.com/locate/compfluid

Two-dimensional simulation of shallow-water waves by Lagrangian block advection

Lai-Wai Tan [a], Vincent H. Chu [b,*]

[a] Faculty of Civil and Environmental Engineering, Universiti Tun Hussein Onn Malaysia, 86400 Batu Pahat, Johor, Malaysia
[b] Department of Civil Engineering and Applied Mechanics, McGill University, 817 Sherbrooke Street West, Montreal, Quebec, Canada H3A 2K6

ARTICLE INFO

Article history:
Received 4 June 2011
Received in revised form 27 February 2012
Accepted 15 April 2012
Available online 24 April 2012

Keywords:
Lagrangian method
Block advection
Shallow-water waves
Capturing shock waves
Tracking wetting-and-drying interface
Positivity of water depth
Discontinuous solutions

ABSTRACT

Waves in shallow water are computed by moving blocks of water in the direction of the flow using a Lagrangian method. The mass and momentum in the displaced-and-deformed blocks after the Lagrangian advection are re-distributed back on to the Eulerian mesh to form new blocks at every increment of time. This Lagrangian block advection guarantees for positive water depth. It also prevents the occurrence of unphysical numerical oscillations. Several numerically challenging problems are considered in a series of simulations using the method. The first problem is the tracking of wetting-and-drying interface in a parabolic bowl. The second problem is the capture of depth and velocity discontinuities across the shock waves. Finally, the block advection method is applied to calculate the flood waves overtopping a meandering river. The results of the simulations are compared with the exact solutions. The convergence of Lagrangian block advection towards the exact solutions is first-order accurate in the simulations of the depth-and-velocity discontinuities.

1. Introduction

Computational stability is crucial to many engineering simulation problems including the flood waves over lands, the evolution of avalanches, the run-up of waves on beaches and the overtopping of water on levees. The computation must capture the discontinuities across the shock waves and the discontinuities at the wave fronts where the wet water meets the dry land. In the classical finite-volume simulations, the discontinuities are the source of unphysical numerical oscillations which often lead the computation to failure. A variety of ad-hoc numerical methods have been developed to manage the computational instability. Shock capture schemes [6,7,26] and flux limiters [10,14,17] have been the methods to control the unphysical numerical oscillations. The advance and the retreat of waters on dry land have been attempted with some success using the wet-and-dry threshold [13,15], the wet cell mapping [9], the artificial porosity techniques [27], the volume-of-fluid method [8,11], the Lagrangian–Eulerian algorithms [1,2,12], and the technique of the artificial viscosity [28,18].

As an alternative to the classical methods, a Lagrangian block advection (LBA) method has been developed by Tan and Chu [22,21] for one-dimensional simulations of water waves in shallow water. In the LBA simulations, the mass and momentum in the water waves are transferred by the Lagrangian advection of the blocks. The LBA method always gives positive water depth. It correctly captures the depth-and-velocity discontinuities while maintaining absolute computational stability. The method has since been applied to a number of one-dimensional (1D) water engineering problems. These include the dam-break waves [21], the collapsing bore [22,19,16], the runup and overtopping of solitary waves [23] and the runup and overtopping of the regular waves [24].

This paper will show how the LBA method is generalized for application to two-dimensional (2D) problems. A couple of 2D analytical solutions involving flow discontinuities is used as the benchmarks. The first of the 2D benchmarks is the solution for water waves in a parabolic bowl by Thacker [25]. The second of the 2D benchmarks is the solution for the shock waves by Stoker [20]. The 2D LBA simulations for these benchmark problems are carried out using progressively smaller block sizes. The convergence is verified by the comparison of the simulations with the analytical solutions. Finally, the versatility of 2D LBA method for engineering application is demonstrated by routing flood waves in a meandering river.

2. Lagrangian block advection

The Lagrangian blocks as the computational elements are defined by the dimensions of the blocks Δx^L and Δy^L and the contents such as volume and momentum in the blocks. Three separate systems of blocks for the volume, $h^L_{i,j}\Delta x^L\Delta y^L$, x-momentums, $u^L_{i,j}\bar{h}^u_{i,j}\Delta x^L\Delta y^L$ and y-momentum $v^L_{i,j}\bar{h}^v_{i,j}\Delta x^L\Delta y^L$, are employed for the LBA simulations on a staggered grid. The superscript 'L'

* Corresponding author.
E-mail address: vincent.chu@mcgill.ca (V.H. Chu).

0045-7930/$ - see front matter © 2012 Elsevier Ltd. All rights reserved.
http://dx.doi.org/10.1016/j.compfluid.2012.04.014

distinguishes the Lagrangian variables from the Eulerian variables. Fig. 1 shows (a) the staggered grid, (b) the volume block, (c) the x-momentum block, and (d) the y-momentum block. As shown in (b–d) of the figure, the blocks initially occupy the same area as the Eulerian cell at the beginning of time step. The contents in the blocks move with the blocks as the blocks are displaced and deformed with the flow. The transfer of the block's contents to its neighboring cells is completed when the old blocks are break up along the grid lines and the new blocks are formed at the end of the Lagrangian advection time step.

Fig. 1b delineates the Lagrangian advection of the volume block. At the beginning of the Lagrangian advection at time t, the edges of the blocks match the Eulerian mesh, i.e.,

$$x^L_{i,j}(t) = x_{i,j}(t),\ y^L_{i,j}(t) = y_{i,j}(t). \tag{1}$$

At the end of the advection at time $t + \Delta t$,

$$x^L_{i,j}(t+\Delta t) = x_{i,j}(t) + \int_0^{\Delta t}\int_0^t a^{xL}_{i,j}\,dt'\,dt, \tag{2}$$

$$y^L_{i,j}(t+\Delta t) = y_{i,j}(t) + \int_0^{\Delta t}\int_0^t a^{yL}_{i,j}\,dt'\,dt. \tag{3}$$

For the waves in shallow-waters, the pressure over the depth may be assumed hydrostatic. The x- and y-components of the depth-averaged flow accelerations are given by the shallow-water equations as follows:

$$a^{xL}_{i,j} = \frac{Du^L_{i,j}}{Dt} = -g\frac{\zeta^L_{i,j} - \zeta^L_{i-1,j}}{\Delta x} + f^x_{i,j}, \tag{4}$$

$$a^{yL}_{i,j} = \frac{Dv^L_{i,j}}{Dt} = -g\frac{\zeta^L_{i,j} - \zeta^L_{i,j-1}}{\Delta y} + f^y_{i,j}, \tag{5}$$

where D/Dt = Lagrangian time-differentiation operator, $\left(u^L_{i,j}, v^L_{i,j}\right)$ = x- and y-components of the flow velocity, $\zeta^L_{i,j} = h^L_{i,j} + z^o_{i,j}$ = water surface elevation, $h^L_{i,j}$ = water depth, $z^o_{i,j}$ = channel bottom elevation, g = gravity, and $\left(f^x_{i,j}, f^y_{i,j}\right)$ = x- and y-components of the other forces such as the friction force. The integrations for the edge co-ordinates of the block, $\left(x^L_{i,j}, y^L_{i,j}\right)$, are carried out using the approximation that the accelerations $\left(a^{xL}_{i,j}, a^{yL}_{i,j}\right)$ are constant throughout the period of the Lagrangian advection from time t to $t + \Delta t$.

Fig. 2 shows how the area of the (i,j)-block is displaced-and-deformed from $\Delta x\Delta y$ to $\Delta x^L\Delta\, y^L$ due the Lagrangian advection. The block occupies initially the same area as the Eulerian cell. The displaced-and-deformed block may occupy an area covering as much as eight neighboring cells as shown. The displaced-and-deformed block is divided along the grid lines into portions and then re-distributed onto the Eulerian mesh to form new blocks at the end of the advection step. A block re-distribution algorithm had been developed to (i) subdivide the old block along the grid lines, (ii) re-distribute the block's content onto its neighboring cells, and (iii) re-construct the new blocks at every time increment. Using the block re-distribution algorithm, the contents in the block are transported across the grid lines from the cell to its neighboring cells. The computational time step must not be too large to cause advection beyond its neighbors. The block re-distribution algorithm was developed by Chu and Altai [4,5] based on a requirement that the displaced-and-deformed block boundary stays within the immediate neighboring cells. This requirement gives a *necessary* condition for the computational stability. Over the period of one Δt, the displacements of all block boundaries $\mathrm{Max}|u_{i,j}|\Delta t$ and $\mathrm{Max}|v_{i,j}|\Delta t$ must not exceed Δx and Δy in the x- and y-directions, respectively. Therefore, The Courant numbers Co_x and Co_y must kept below the value of unity during the computation as follows:

$$\mathrm{Co}_x = \frac{\mathrm{Max}|u_{i,j}|\Delta t}{\Delta x} < 1, \tag{6}$$

$$\mathrm{Co}_y = \frac{\mathrm{Max}|v_{i,j}|\Delta t}{\Delta y} < 1. \tag{7}$$

These necessary conditions for stability would keep the time step Δt sufficiently small so that the deformation in one advection step would not be excessive to cause *Lagrangian entanglement*. The area of the block $\Delta x^L_{i,j}\Delta y^L_{i,j}$ may become negative after the Lagrangian advection if the edge on one side of the block overtakes the other side from behind.

The third necessary condition for the computational stability is the Courant–Friedrichs–Lewy (CFL) condition for the shallow-water waves:

$$\mathrm{Co}_c = \frac{\sqrt{g\mathrm{Max}|h_{i,j}|}\Delta t}{\Delta x} < 1, \tag{8}$$

where $\sqrt{g\mathrm{Max}|h_{i,j}|}$ is the wave speed of the shallow-water waves. The time step must be selected to meet all three necessary conditions as given by the formula:

$$\Delta t = \mathrm{Min}\left\{\frac{\Delta x}{\sqrt{g\mathrm{Max}|h_{i,j}|}}, \frac{\Delta x}{\mathrm{Max}|u_{i,j}|}, \frac{\Delta y}{\mathrm{Max}|v_{i,j}|}\right\}\mathrm{Co}. \tag{9}$$

According to this formula, the time step Δt is proportional to the Courant number Co. The necessary condition for computational stability is $\mathrm{Co} < 1$.

As the stability, the accuracy of the Lagrangian advection also depends on the time step size and Co. Since the value of $\mathrm{Co} = 0.2$ was used in most of the computations carried out using the classical finite-volume (CFV) method, the same value $\mathrm{Co} = 0.2$ is selected for the present series of LBA simulations. With this selection, the results of the present LBA simulations are comparable with the results obtained using the CFV method.

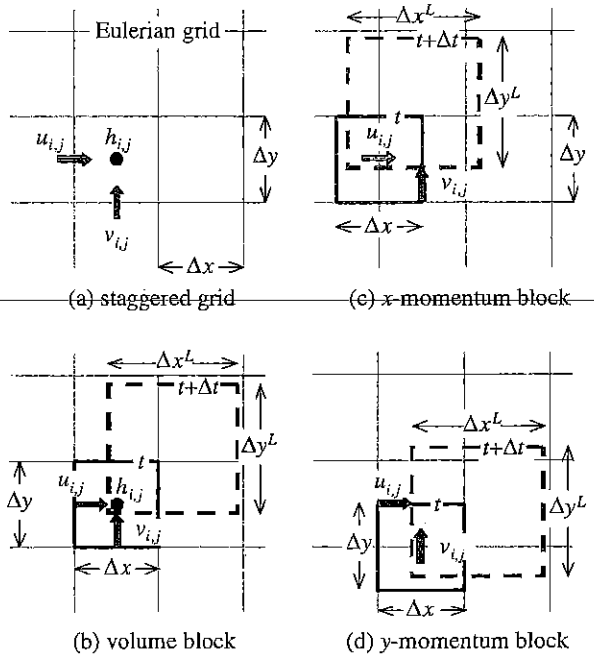

Fig. 1. (a) The staggered grid, (b) the volume blocks, (c) the x-momentum blocks, and (d) the y-momentum blocks. The solid rectangles show the blocks before the Lagrangian advection. The dashed rectangles delineate the edges of the blocks after the Lagrangian advection.

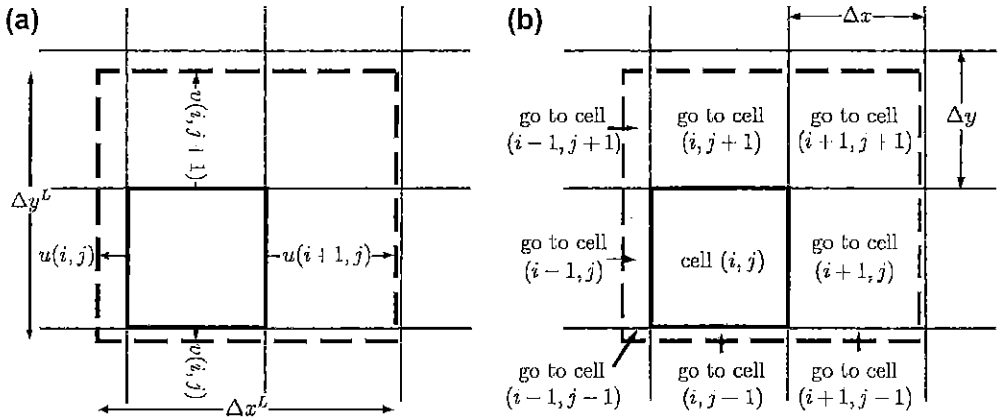

Fig. 2. The subdivision of the displaced-and-deformed Lagrangian block into portions along the grid lines and the re-distribution of the block's content on to the Eulerian cells [4,5]. (a) The block initially occupies the same area as the Eulerian cell (solid rectangle) at the start of the Lagrangian advection. The displaced-and-deformed block (dashed rectangle) may occupy as much as eight neighboring cells at the end of the Lagrangian advection time step. (b) The re-distribution of the contents in the displaced-and-deformed block on to its neighboring cells.

The contents in the blocks may or may not be constant during the Lagrangian advection. Since the water is incompressible, the volume in the block is constant during the advection, i.e.,

$$\frac{D}{Dt}\left[h^L_{i,j}\Delta x^L_{i,j}\Delta y^L_{i,j}\right] = 0. \tag{10}$$

The re-distribution algorithm does not change the overall content in the blocks. Therefore, the volume in the block is conservation during the Lagrangian advection. The overall volume also is conserved during the subsequent re-distribution of the volume among the blocks.

The computations for the momentum blocks follow the same procedure as the volume blocks. However, the momentums are changed by the forces acting on the momentum blocks as follows:

$$\frac{D}{Dt}\left[u^L_{i,j}\bar{h}^u_{i,j}\Delta x^L_{i,j}\Delta y^L_{i,j}\right] = -g\bar{h}^u_{i,j}\frac{\zeta^L_{i,j}-\zeta^L_{i-1,j}}{\Delta x} + \bar{h}^u_{i,j}f^x_{i,j}, \tag{11}$$

$$\frac{D}{Dt}\left[v^L_{i,j}\bar{h}^v_{i,j}\Delta x^L_{i,j}\Delta y^L_{i,j}\right] = -g\bar{h}^v_{i,j}\frac{\zeta^L_{i,j}-\zeta^L_{i,j-1}}{\Delta y} + \bar{h}^v_{i,j}f^y_{i,j}, \tag{12}$$

where $\bar{h}^u_{i,j} = \frac{1}{2}\left(h^L_{i-1,j} + h^L_{i,j}\right)$ = the depth in the u-block and $\bar{h}^v_{i,j} = \frac{1}{2}\left(h^L_{i,j} + h^L_{i,j-1}\right)$ = the depth in the v-block. The first term on the right hand side of the equations is the hydrostatic pressure force. The second term on the right hand side is the friction forces, which has been ignored for simplicity in all simulations presented in this paper.

The most significant advantage of this 2D LBA method is computational stability. The method ensures positive water depth. Unphysical numerical oscillation is not possible even in region of steep gradients near the flow discontinuities. The application of the method to shallow-water waves is demonstrated through a series of simulations of the flow discontinuities to be presented in the subsequent sections.

3. Water waves in a parabolic bowl

The first series of the 2D LBA simulations was carried out for the standing waves of water inside a parabolic bowl. Fig. 3 shows the blocks of water when very large blocks are used in the simulation. Standing wave motion is produced by a parabolic mound of water, which moves up and down under the influence of the gravity. The analytical solution of this problem for non-breaking waves of small amplitude in shallow water was due to Thacker [25]. Fig. 4 shows the LBA simulation results of the standing waves of maximum height $(h_o)_{max} = 1.72$ m in a parabolic bowl of 4000 m radius. The analytical solution of Thacker was closely reproduced by the LBA simulation when the sufficiently small block size of $\Delta x = \Delta y = 5$ m was used in the simulation.

The water in the bowl is initially at rest. The gravity potential energy is maximum at the initial position when the time $t = 0$. As the water in the bowl starts to fall under the influence of the gravity, kinetic energy of the water increases at the expense of the potential energy. The kinetic energy of the water in the bowl reaches its maximum as water moves downward to the lowest position at time $t = \frac{T}{2}$. The entire process repeats itself after one wave period T of the standing wave. The velocity is zero initially at time $t = 0$ and is again zero after one-half of one wave period at the time $t = \frac{T}{2}$ and after one wave period at the time $t = T$.

As shown in the middle column of the figure, the velocity distribution across the bowl is linear. The maximum of the velocity is at the wave front where the wet water meets the dry surface of the bowl. The discontinuity of the velocity at the wave front would be most difficult to be simulated by the classical finite-volume method. Remarkably, this discontinuity is perfectly simulated by the Lagrangian block advection without encountering any numerical oscillations. With this stability of the computation, infinite cycles of the advance and recede of the wet water on the dry surface of the bowl were simulated by the LBA in perpetuity without interruption.

Although the stability of the computation is assured, the total (potential plus kinetic) energy of the water in the bowl, E, is not exactly constant. A detectable dissipation of total energy, E, is observed over the 18 wave-period of simulation as shown in Fig. 5a. Since friction is not included in the formulation, this energy dissipation is not physical and is due to the inaccuracy of the computation. Simulations were carried out for the progressively reduced block sizes varying from $\Delta x = \Delta y = 80$ m to $\Delta x = \Delta y = 40$ m, 20 m, 10 m and 5 m. The dimensionless rate of the dissipation over one wave period, $(T/E_o)\Delta E/\Delta t$, was determined as the parameter to measure the computation error. The correlation of this error parameter with the block size $\Delta x/(h_o)_{max}$ is shown Fig. 5b, which shows the error approaches zero as the simulation approaches the exact solution. The convergence to the exact solution is first order with the value of $p \simeq 1$ using the error-estimation method recommended by Celik et al. [3]. Higher oder of accuracy is achievable and has been reported. Using an Eulerian–Lagrangian scheme,

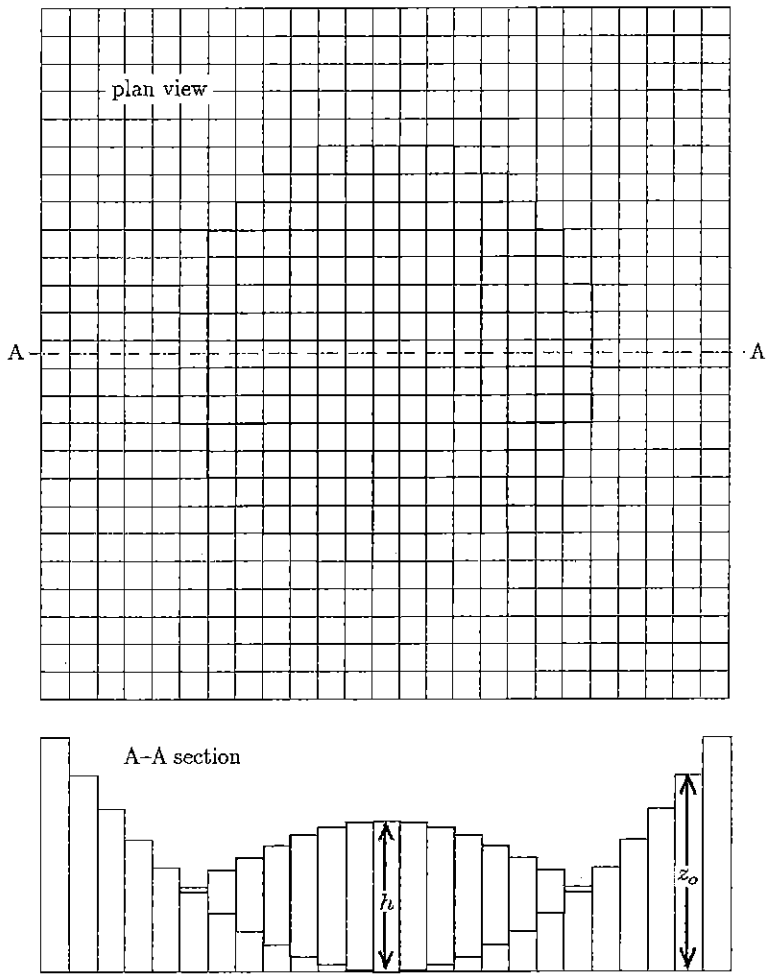

Fig. 3. The wetting and drying of the surface of a parabolic bowl produced by a parabolic mound of water under the gravity. The block sizes are $\Delta x = \Delta y = 3.2$ m in a bowl of 40 m radius. The crest height of the initial mound of water is $(h_o)_{max} = 0.02$ m.

Bokhove [2] were able to obtained second-order accuracy in tracking the wetting and drying at the wave front.

4. Oblique shock wave

The second series of LBA simulations was designed to examine the shock capture capability of the method. Oblique shock waves were produced in a 100 m × 100 m square basin by the sudden removal of a dam in the diagonal direction. Initially, the water depth was $h_o = 10$ m on one side of the dam and was $h_d = 1$ m on the other side. Shock waves were produced in the basin immediately after the removal of the dam. Fig. 6a–c show the propagation and the reflection of the shock waves at time $t = 0.01$ s, 2.5 s and 4 s, respectively. The computation was carried out using a block size $\Delta x = \Delta y = 0.04$ m. The accuracy of the simulation was determined by comparing the simulations with the analytical solution of Stoker [20]. Fig. 6d and e show the shock-wave depth and velocity profiles along a section A–A at time $t = 2.5$ s. The analytical solution of Stoker [20] gives the height of the shock wave to be $(h_s)_{Stoker}/h_o = 0.396$ and the velocity of the shock wave to be $(u_s)_{Stoker}/\sqrt{gh_o} = 0.741$ at this time $t = 2.5$ s. These height and velocity of the shock were accurately determined by the LBA simulation in excellent agreement with the exact solution of Stoker [20]. While the oblique shock waves are simulated by the LBA method without interruption, the accuracy of the results nevertheless are dependent on the size of the block. Improvement to the accuracy of the simulation is possible as the block size is reduced. Fig. 7a–c show the fractional errors and their relation to the block size $\Delta x (=\Delta y)$. Using Stoker's [20] analytical solution as the benchmark, the fractional errors for the shock-wave position, the shock-wave height and shock-wave velocity are:

$$\frac{x_s - (x_s)_{Stoker}}{(x_s)_{Stoker}}, \quad \frac{h_s - (h_s)_{Stoker}}{(h_s)_{Stoker}}, \quad \text{and} \quad \frac{u_s - (u_s)_{Stoker}}{(u_s)_{Stoker}}. \tag{13}$$

These fractional errors are plotted in the logarithmic scales in Fig. 7a–c. As shown in these figures, the simulations approach the exact solution following the order of accuracy of $p \simeq 1$, $p \simeq 2$, and $p \simeq 1$ for the location, depth and velocity, respectively. The p-values were determined using the definition introduced by Celik et al. [3]. The formal order of accuracy for the LBA simulations of the shock waves is not entirely clear. The LBA formulation does not follow the classical order of approximation. Nevertheless, the orders of accuracy obtained from the LBA simulations of the shock wave are consistent with the assessment by Godunov [6] on the discontinuous solutions of the shallow-water equations.

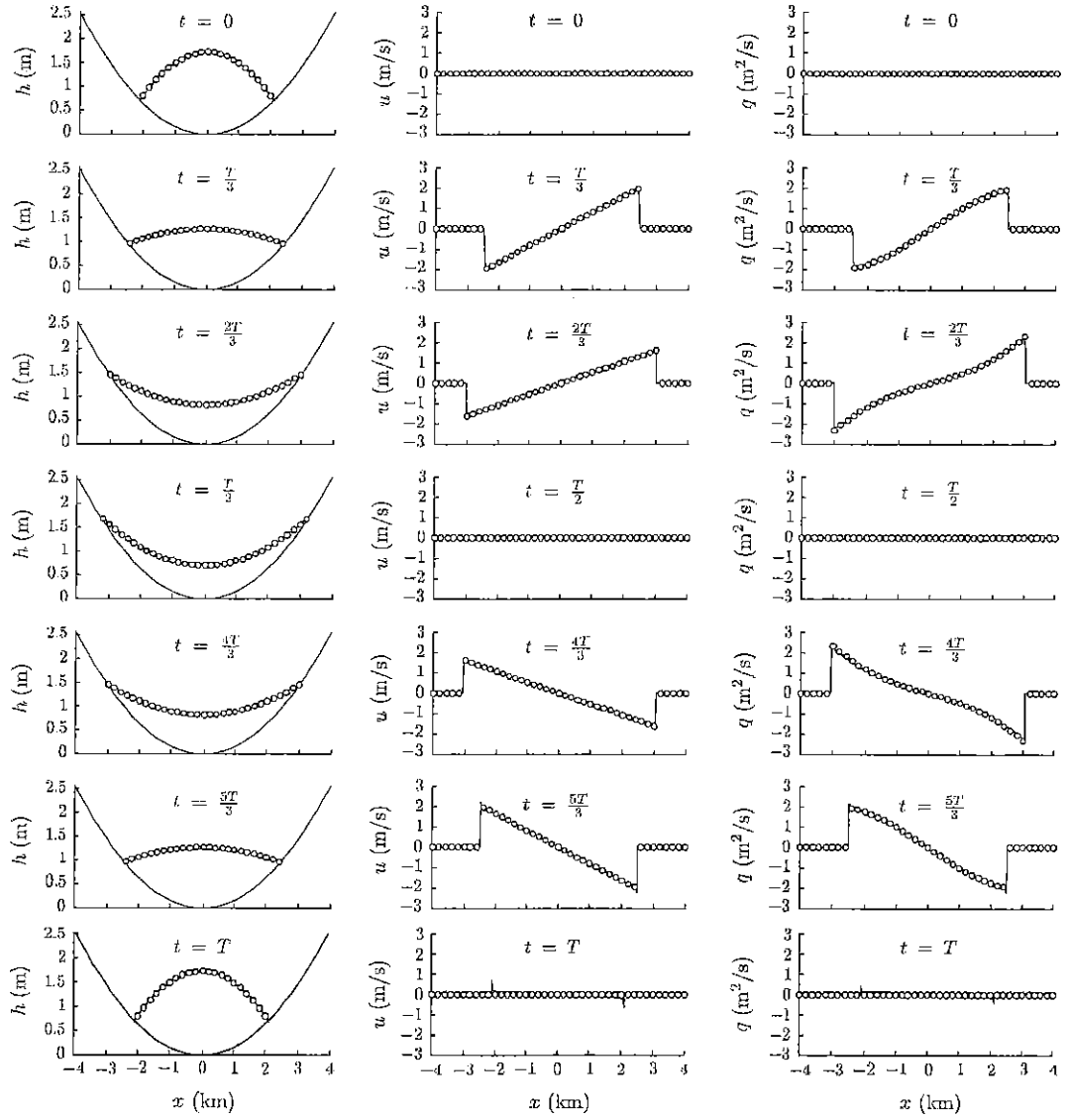

Fig. 4. Depth h (left-hand-side column), velocity u (middle column) and discharge $q = uh$ (right-hand-side column) profiles at time $t = 0$, $t = \frac{T}{3}$, $t = \frac{2T}{3}$, $t = \frac{T}{2}$, $t = \frac{4T}{3}$, $t = \frac{5T}{3}$, and $t = T$. The Lagrangian block advection simulations was obtained using the block sizes of $\Delta x = \Delta y = 5$ m. The initial maximum depth of the parabolic mound of water at rest is $(h_o)_{max} = 1.72$ m. The radius of the parabolic bowl is 4000 m. The solid lines denote the block advection simulation profiles on the plane of symmetry. The circle symbol denotes the analytical solution of Thacker [25].

Fig. 8 shows the total potential energy and total kinetic energy in the 100-m × 100-m basin and their variations with time. The LBA simulation of the shock waves is absolutely stable. As the shock waves of diminishing amplitude are reflected back and forth across the basin, more than 90% of the energy are dissipated over the period of 100 s.

5. Flood waves overtopping a meandering river

The final series of 2D LBA simulations was carried out for flood waves in an idealized meandering river. The calculations was conducted for a 10 m wide river of 1 m water depth. The meander wave length is 50 m and the meander amplitude is 5 m as shown in Fig. 9. Periodic boundary conditions are imposed every 150 m to produce the equivalent river of infinite length. The elevation of the floodplain is 2 m higher than the river bed. The water is accelerated from rest until the flow through the river reaches a quasi-steady state. Fig. 10 shows the vorticity profiles of the quasi-steady flow through the meander for a range of channel slopes varying from $S_o = -dz_o/dx = 0.0025$ to $S_o = 0.005$, 0.01, and 0.02. The flow is sub-critical when the channel has a small slope of $S_o = 0.0025$. Part of the flow becomes super-critical as the velocity in the channel increase with the slope. The flow is primarily super-critical when the channel has a large slope of $S_o = 0.02$.

The sub-critical shear flow is characterized by the formation of the eddies as the flow negotiates through the meander. The super-critical flow on the other hand is dominated by the shock waves and the energy dissipation by the shock waves. The conveyance resistance produced by the eddies and the shock waves in the meander has been examined in some details by Wang et al. [29]. The simulations by Wang et al. however were carried out using the classical finite-volume (CFV) formulation. Fig. 10 shows the

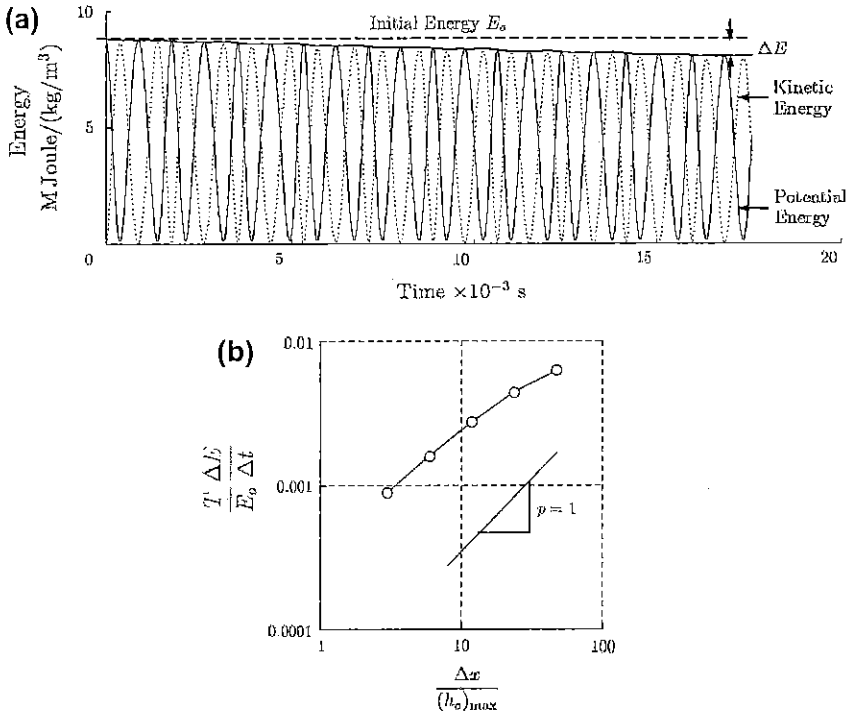

Fig. 5. (a) The potential and kinetic energies of water waves in the parabolic bowl calculated by LBA using $\Delta x = \Delta y = 5$ m over the period of 18 wave cycles. (b) Dimensionless dissipation error $(T/E_o)\Delta E/\Delta t$ correlated with the block size $\Delta x/(h_o)_{max}$; $\Delta x = \Delta y = 5$ m, 10 m, 20 m, 40 m and 80 m.

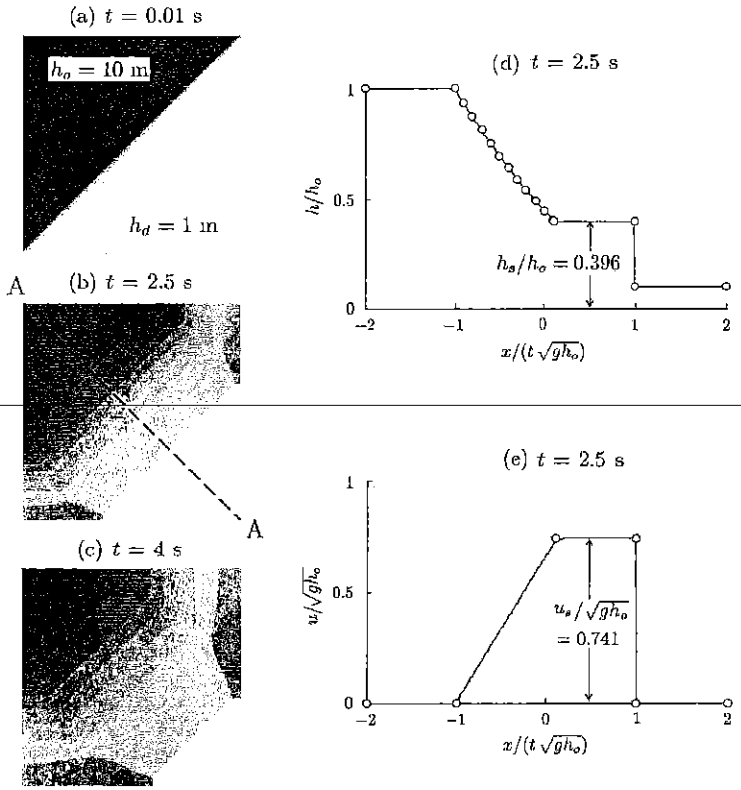

Fig. 6. Dam-break shock waves in a 100-m × 100-m square basin computed by the Lagrangian block-advection using $\Delta x = \Delta y = 0.04$ m. (a–c) Water depth contours at time $t = 0.01$ s, 2.5 s and 4 s, respectively. (d) Water depth and (e) velocity profiles in the cross section A–A perpendicular to the shock wave at time $t = 2.5$ s. The lines denote the LBA simulations and the circles denote the exact solution of Stoker [20].

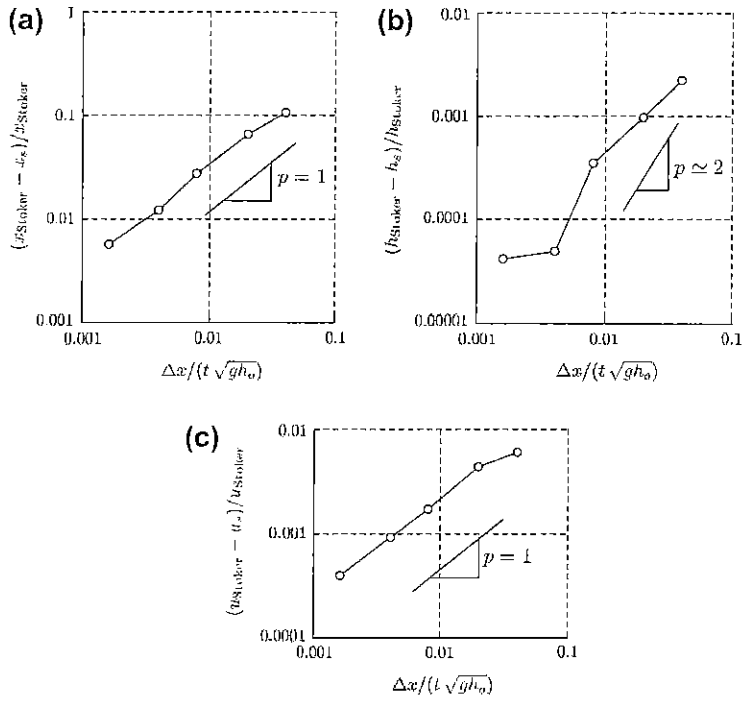

Fig. 7. Fractional computation errors for (a) the shock-wave position, (b) the shock-wave height, and (c) the shock-wave velocity obtained by the LBA method for the block sizes $\Delta x = 1$ m, 0.5 m, 0.2 m, 0.1 m and 0.04 m.

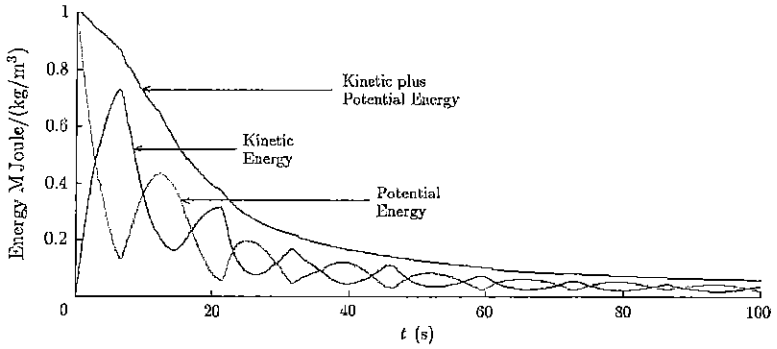

Fig. 8. Energy dissipation as the shock waves are reflected back and forth across the 100-m × 100-m square basin.

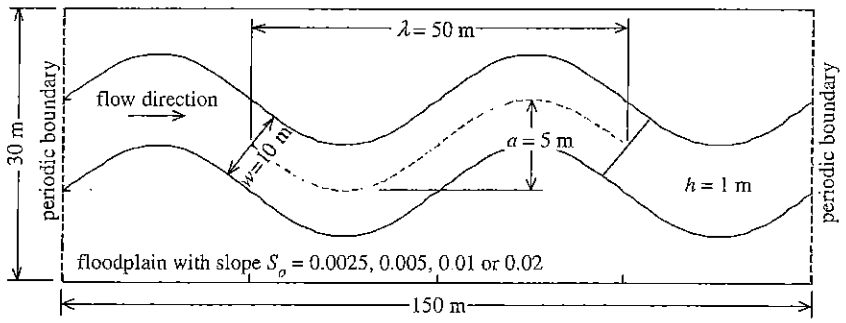

Fig. 9. An idealized river of 10 m wide on a meander wave length of 50 m and a meander amplitude of 5 m. The floodplain is 2 m higher in elevation than the meander river's bed.

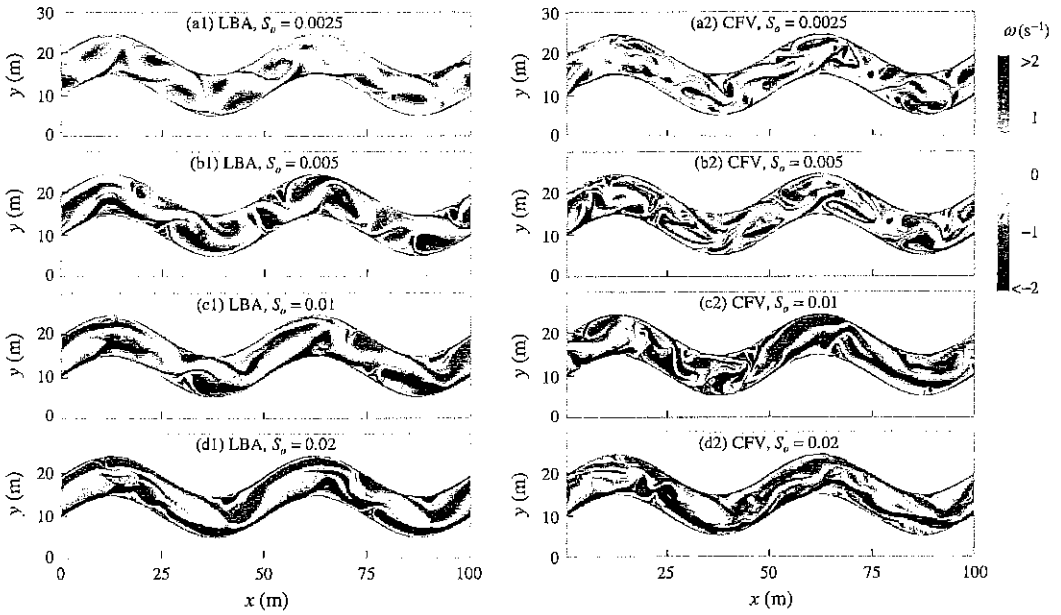

Fig. 10. Vorticity profiles for the quasi-steady state flow through the meander river of bed slopes $S_o = 0.0025$, 0.005, 0.01, and 0.02 obtained using the LBA method (left) and the CFV method (right).

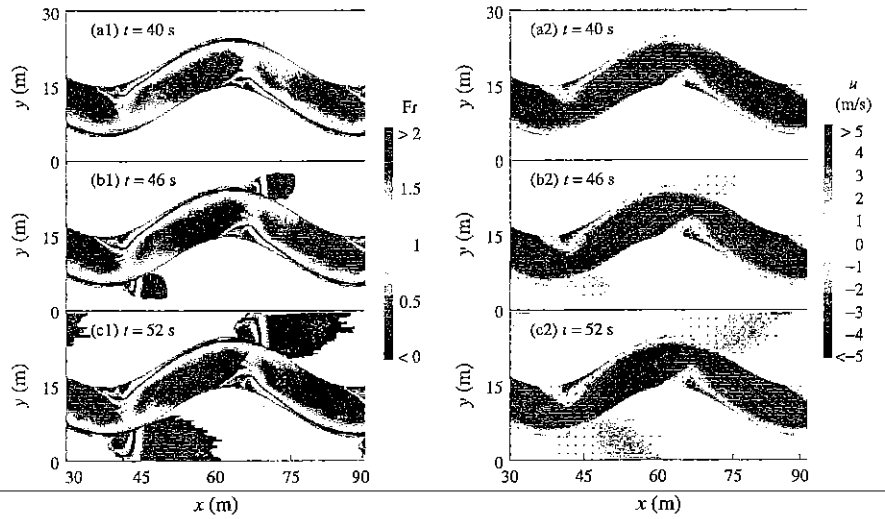

Fig. 11. Froude number profiles (left) and u-velocity profiles (right) at the instance shortly after the meander river overtop it's bank. The flow changes from sub-critical (Fr < 1) to super-critical (Fr > 1) across the shock waves. The channel bottom slope $S_o = 0.02$.

comparison between the vorticity profiles obtained using the LBA method and CFV method. The LBA results are shown on the left hand side of the figure and the CFV results on the right hand side of the figure. While the LBA simulation are more stable, the CFV results are more refined and possibly more accurate. However, the computer-usage time of the CFV simulation is three to four time greater partly because the need to use the flux limiter to control the unphysical numerical oscillations. Given a fixed computer resource, the LBA simulations can afford using a finer block size than the CFV calculations of the same problem. So, the accuracy of the LBA computation can be improved by using smaller block size. The stability of the computation is not always possible when using the CFV method. Although the flux limiter is effective in minimizing the unphysical numerical oscillations, it does not guarantee for positive water depth. In fact, the negative water depth is the most common cause for the failure of the computation. At the wave front where the wet water meets the dry land, very small numerical oscillations can lead to negative water depth and the catastrophic collapse of the computation using the CFV method.

The fact that the overtopping of the river waters onto the floodplain can be simulated is entirely due to the computational stability of the LBA method. Fig. 11 shows the LBA simulations on a steep slope $S_o = 0.02$ at the time $t = 40$ s, 46 s and 52 s when the flood waves begins to advance onto the dry floodplain. On this steep slope, the flow is super-critical in which the Froude number of the flow is greater than unity in the central region of the river.

The computation using the LBA method has captured the shock waves and as well the wave front of the wet water on the dry floodplain. Clearly, the computational stability is a significant advantage. The abrupt 2 m change in the bottom elevation at the edge between the idealized river and the floodplain has not interrupted the LBA computations. The simulation of the river waters overtopping its bank would be a difficult problem, and the wetting-and-drying treatment [2,15,12,11] would be required if the CFV method were employed in the simulations. In contrast, the LBA simulation of the floods is simple as the treatment for the wetting and drying is not necessary using the LBA method. The simplicity in the implementation and the stability of the 2D LBA method are advantageous in dealing with the floods through erodible rivers. The erosion at the wave front may need a three-dimensional model. However, stable 2D LBA simulations always can be carried out with certainty even when the floods are negotiating through the complex terrain of a realistic river valley.

6. Conclusions

The two-dimensional Lagrangian block advection (2D LBA) method has been developed for the computation of the shallow-water waves. A series of simulations using progressively refined block sizes has been carried out. The convergence to the exact solutions for the two benchmark problems follows approximately the first-order accuracy, which is consistent with the assessment by Godunov [6] on the discontinuous solutions of the shallow-water equations. The LBA method is distinguished from the classical method for its ability to capture discontinuities without sacrifices the computational stability and accuracy. The classical finite-volume (CFV) method of estimating the fluxes using the truncated series is not accurate in the regions where the depth and velocity change rapidly. The error due to the series truncation has been the source of unphysical numerical oscillations and computational instability at the discontinuities. The LBA method on the other hand is not dependent on the fluxes. Therefore, the steep gradients near the discontinuities are not adversely affecting the accuracy and the stability of the LBA simulations. A number of applications to water-engineering problems had been carried out recently to take advantage of the computational stability of the LBA methods. These include the 2D LBA simulations of turbulent flows by Chu and Altai [4,5] and the series of 1D simulations for the dam-break waves, the waves on beaches and the waves overtopping of levee by Tan and Chu [21–24]. Chu and Altai [4,5] conducted the 2D LBA simulations of turbulent flow using the vorticity-and-stream-function formulation. The present 2D LBA simulation method for the shallow-water waves was developed based on the primitive-variable formulation.

References

[1] Akanbi AA, Katopodes ND. Model for flood propagation on initially dry land. J Hydr Eng 1988;114(7):689–706.

[2] Bokhove O. Flooding and drying in finite-element Galerkin discretizations of shallow-water equations. Part I: One dimension. J Sci Comput 2005;22:47–82.

[3] Celik IB, Ghia U, Roache PJ, Freitas CJ, Coleman H, Raad PE. Procedure for estimation and reporting of uncertainty due to discretization in CFD applications. J Fluid Eng 2008;130:1–4.

[4] Chu VH, Altai W. Simulation of shallow transverse shear flow by generalized second moment method. J Hydr Res 2001;39(6):575–82.

[5] Chu VH, Altai W. Simulation of turbulence and gravity interfaces by Lagrangian block method. In: Armfield S, Morgan P, Srinivas K, editors. Computational fluid dynamics. Germany: Springer; 2002. p. 299–304.

[6] Godunov SK. A difference scheme for numerical solution of discontinuous solution of hydrodynamic equations. Math Sb 1959;47:271–306.

[7] Harten A. High resolution schemes for hyperbolic conservation laws. J Comput Phys 1983;49(3):357–93.

[8] Hirt CW, Nichols BD. Volume of fluid (VOF) method for the dynamics of free boundaries. J Comput Phys 1981;39(1):201–25.

[9] Ji Z-G, Morton MR, Hamrick JM. Wetting and drying simulation of estuarine processes. Estuar, Coast Shelf Sci 2001;53:683–700.

[10] Kemm F. A comparative study of TVD-limiters - well-known limiters and an introduction of new ones. Int J Numer Meth Fluids; 2010 doi: 10.1002/fld.2357.

[11] Larmaeia MM, Mahdi T-F. Simulation of shallow water waves using VOF method. J Hydro-environ Res 2010;3(4):208–14.

[12] Liang Q, Marche F. Numerical resolution of well-balanced shallow water equations with complex source terms. Adv Water Res 2009;32:873–84.

[13] Leendertse JJ. A water-quality simulation model for well-mixed estuaries and coastal seas: Volume I, Principles of computation. Santa Monica: Rand; 1970.

[14] Leonard BP. Simple high-accuracy resolution program for convective modelling of discontinuities. Int J Numer Meth Fl 1988;8:1291–318.

[15] Marche F. A simple well-balanced model for two-dimensional coastal engineering applications. In: Benzoni-Gavage S, Serre D, editors. Hyperbolic problems: theory, numerics, applications. Berlin Heidelberg, Heidelberg: Springer; 2008. p. 271–83.

[16] Peregrine DH, Williams SM. Swash overtopping a truncated plance beach. J Fluid Mech 2001;440:391–9.

[17] Pinilla CE, Bouhairie S, Tan L-W, Chu VH. Minimal intervention to simulations of shallow-water equations. J Hydro-Environ Res 2010;3(4):201–7.

[18] Roeber V, Cheung KF, Kobayashi MH. Shock-capturing Boussinesq-type model for nearshore wave processes. Coas Eng 2010;57(4):407–23.

[19] Shen MC, Meyer RE. Climb of a bore on a beach: Part 3. Run-up. J Fluid Mech 1963;16:113–25.

[20] Stoker JJ. Water Waves: the mathematical theory with applications. New York: Wiley Interscience; 1957.

[21] Tan L-W, Chu VH. Simulation of wave fronts on dry beds using Lagrangian blocks. Eng Comput Mech 2009;162(2):57–66.

[22] Tan L-W, Chu VH. Wet-and-dry interface on steep slopes simulations using Lagrangian blocks. In: Chistodoulou, Stampu, editors. Environmental hydraulics. London: Taylor & Francis; 2010. p. 997–1002. ISBN 978-0-415-58475-3.

[23] Tan LW, Chu VH. Wave runup simulations using Lagrangian blocks on Eulerian mesh. J Hydro-Environ Res 2010;4(part 2):193–200.

[24] Tan L-W, Chu VH. Regular periodic waves runup and overtopping simulations by Lagrangian blocks. In: Proceedings of the 32nd coastal engineering conference, vol. 32; 2011. p. 15. <http://journals.tdl.org/ICCE/issue/view/154>.

[25] Thacker WC. Some exact solutions to the nonlinear shallow-water wave equations. J Fluid Mech 1981;107.

[26] Toro EF. Shock capturing methods for free surface flows. Toronto: Wily. p. 309.

[27] van't Hof B, Vollebregt EAH. Modelling of wetting and drying of shallow water using artificial porosity. Int J Numer Meth Fluids 2005;48(11):1199–217.

[28] Von Neumann J, Richtmyer RD. A method for the numerical calculation of hydrodynamic shocks. J Appl Phys 1950;21:232–7.

[29] Wang T, Tan L-W, Chu VH. Flood-waves simulation by classical method of consistent transport. In: Kuzmin A, editor. Computational fluid dynamics 2010 ICCFD6. Springer; 2011. p. 287–96. ISBN 3642178839.